

Synthesis, structure, Hirshfeld analysis and fluorescence properties of a new asymmetric salamo-based ligand and its Cu(II) complex involving oxime oxygen coordination

Xin Xu , Ji-Fa Wang , Ruo-Nan Bian & Li Zhao

To cite this article: Xin Xu , Ji-Fa Wang , Ruo-Nan Bian & Li Zhao (2020): Synthesis, structure, Hirshfeld analysis and fluorescence properties of a new asymmetric salamo-based ligand and its Cu(II) complex involving oxime oxygen coordination, Journal of Coordination Chemistry, DOI: [10.1080/00958972.2020.1822524](https://doi.org/10.1080/00958972.2020.1822524)

To link to this article: <https://doi.org/10.1080/00958972.2020.1822524>



Published online: 19 Sep 2020.



Submit your article to this journal [↗](#)



Article views: 17



View related articles [↗](#)



View Crossmark data [↗](#)



Synthesis, structure, Hirshfeld analysis and fluorescence properties of a new asymmetric salamo-based ligand and its Cu(II) complex involving oxime oxygen coordination

Xin Xu, Ji-Fa Wang, Ruo-Nan Bian and Li Zhao

School of Chemical and Biological Engineering, Lanzhou Jiaotong University, Lanzhou, Gansu 730070, People's Republic of China

ABSTRACT

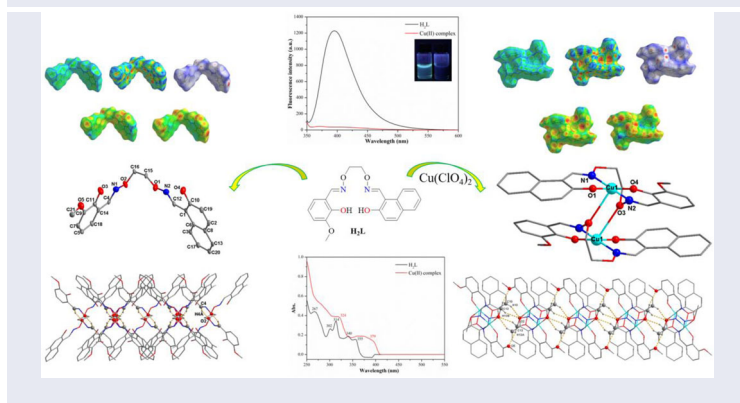
A new asymmetric salamo-based ligand (H_2L) was synthesized and upon reaction with $Cu(ClO_4)_2$ an extremely rare dinuclear Cu(II) complex $[Cu_2(L)_2]$ was formed and characterized by elemental analyses, infrared spectroscopy, UV–vis absorption spectroscopy, X-ray single crystal diffraction and Hirshfeld surface analyses. The Cu(II) complex consists of two Cu(II) ions and two fully deprotonated ligand (L^{2-}) units. The Cu(II) is coordinated with the N_2O_2 cavity (N1, N2, O1 and O4) of L^{2-} and the oxime oxygen (O3) of another L^{2-} unit to form a uncommon dinuclear structure. The Cu(II) is five-coordinated, $\tau = 0.02$, and has a configuration of slightly twisted tetragonal pyramidal geometry. The comparison between H_2L and its Cu(II) complex through Hirshfeld surface analyses shows that the interaction of O–H/H–O is reduced, indicating that deprotonation of phenolic hydroxyl group and the coordination of Cu(II) forms a stable complex. In addition, fluorescence quenching of the Cu(II) complex compared to H_2L further confirms the above experimental results.

ARTICLE HISTORY

Received 8 July 2020
Accepted 31 August 2020

KEYWORDS

Salamo-based ligand; Cu(II) complex; synthesis; crystal structure; Hirshfeld surface analysis



1. Introduction

Although salen-based compounds have been synthesized long ago, as a significant class of chelating ligands, they have been one of the research hotspots in the field of coordination chemistry [1–6]. Such compounds have a special N_2O_2 coordination environment, and N and O have strong electron donating ability [7, 8], so different metal ions can be embedded to form metal complexes with novel structures and different properties [9–14]. Such metal complexes are constructed from salen-based ligands and are widely used in nonlinear optical materials [15–17], molecular probes [18, 19], magnetic materials [20–22], antibacterial activities [23, 24], and electrochemistry [25, 26]. Salen-based ligands have many excellent properties [27–30], but they are prone to hydrolysis, so it is difficult to prepare asymmetric salen-based ligands [31–34].

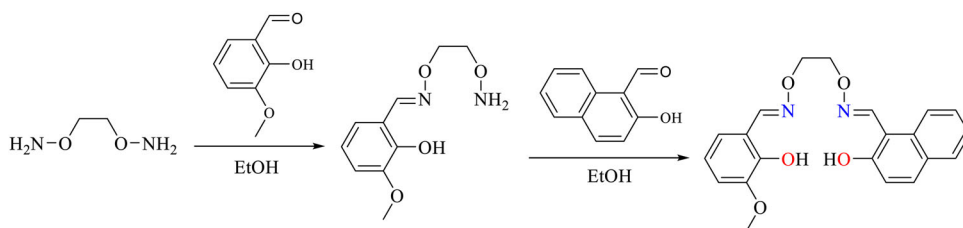
Salamo-based ligands are derivatives of salen-based ligands [35–38]. By introducing an oxygen into the ethylenediamine structure [39–44], the stability of the ligand is improved, so it has a broad development space [45–47]. In recent years, the research focus has been on the synthesis and properties of salamo-based ligands and their new complexes [48–51]. Salamo-based ligands usually lose two or more hydrogens for metal coordination, thus forming stable complexes with metal ions [52, 53]. Therefore, the study of salamo-based complexes has research value and application prospects [54–57]. These results have enabled salamo-based compounds to make significant progress and breakthroughs in the fields of sensors [58–60] and supramolecular structures [61, 62]. For example, salamo-based compounds can identify metal ions in the physiological environment; this quantitative identification method has important application value in environmental monitoring [63–66]. Meanwhile, formation of supramolecular network structures has a greater impact on the coordination environment and fluorescence properties of the obtained complexes, which makes the research more valuable [49, 61].

In the existing salamo-based complexes, there are relatively few metal complexes in which oxime oxygens participate in coordination [67]. In this article, a new salamo-based ligand was synthesized and single crystals of the ligand were obtained. An uncommon Cu(II) complex of the ligand was obtained in which the oxime oxygen participates in coordination.

2. Experimental

2.1. Materials and physical measurements

2-Hydroxy-3-methoxybenzaldehyde and salicylaldehyde were purchased from Shanghai Merery Company with a purity of 98%. The solvents required for other experiments were purchased from Tianjin Chemical Reagent Factory. The GmbH VarioEL V3.00 automatic element analyzer was used for C, H, and N analysis. Elemental analysis of Cu(II) was performed using an IRIS ER/S-WP-1 ICP atomic emission spectrometer. The 1H -NMR spectra were measured on a Bruker AV 500 MHz spectrometer. Melting points were measured by a micro melting point instrument manufactured by Beijing Tektronix Instrument Co., Ltd. FTIR spectra were obtained by using KBr (500 – 4000 cm^{-1}) and CsI (100 – 500 cm^{-1}) pellets on a VERTEX70 FTIR



Scheme 1. Synthetic route to H_2L .

spectrophotometer (Bruker, Billerica, MA, USA). UV–visible absorption and fluorescence spectra were determined using Shimadzu UV-3900 (Shimadzu, Japan) and Hitachi F-7000 (Hitachi, Tokyo, Japan) spectrometers, respectively. The 1 cm quartz cuvette and Xe lamp were used as light source to record the fluorescence spectrum. X-ray single crystal structures were measured on a Bruker Smart Apex CCD diffractometer. The Crystal Explorer program was used for Hirshfeld surface analysis of the Cu(II) complex, all according to methods previously reported.

2.2. Preparation of H_2L

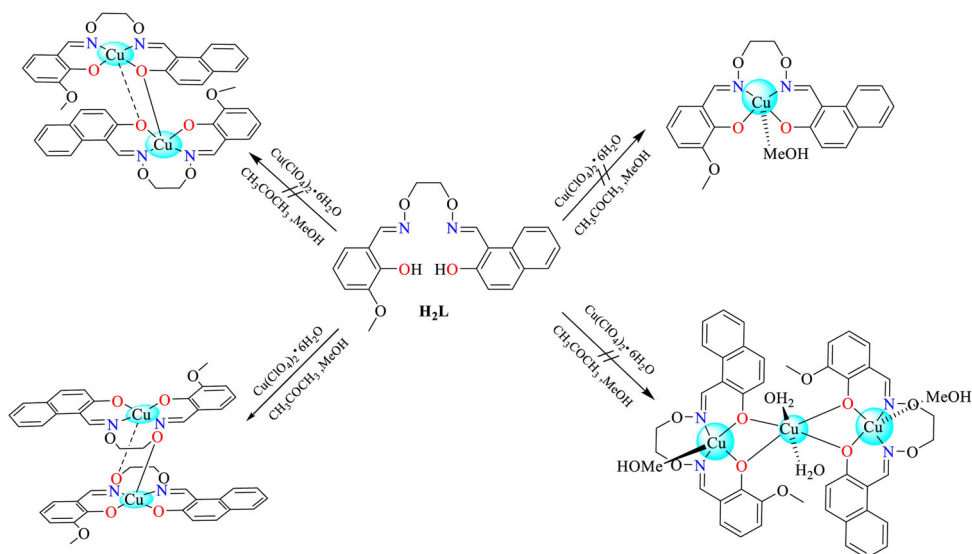
The synthetic route to H_2L is shown in Scheme 1. 1,2-Bis(aminooxy)ethane was synthesized following the previously reported procedure [35, 37]. In an ethanol solution (20 mL) of 2-hydroxy-3-methoxybenzaldehyde (3.0 mmol, 456.39 mg) was slowly added 1,2-bis(aminooxy)ethane (3.0 mmol, 272.6 mg) in absolute ethanol (20 mL). The solution was stirred for 5–6 h with a magnetic stirrer, the solution was concentrated in vacuo, and 6-methoxy-2-[O-(1-ethoxyamide)]oxime-1-phenol was separated by column chromatography. The obtained ethanol solution of 6-methoxy-2-[O-(1-ethoxyamide)]oxime-1-phenol (2.0 mmol, 448.06 mg) was reacted directly with 2-hydroxy-1-naphthaldehyde (2.0 mmol, 344.36 mg) by the one-pot method to obtain H_2L . The yield is 55.3% (based on 2-hydroxy-1-naphthaldehyde). m.p.: 113–115 °C. Anal. Calcd for $C_{21}H_{20}N_2O_5$: C, 66.31; H, 5.30; N, 7.36. Found: C, 61.52; H, 5.37; N, 7.28. 1H -NMR (500 MHz, $CDCl_3$): δ 10.82 (s, 1H), 9.80 (s, 1H), 9.18 (s, 1H), 8.28 (s, 1H), 7.97 (d, J = 8.5 Hz, 1H), 7.78 (s, 2H), 7.51 (s, 1H), 7.36 (t, J = 7.1 Hz, 1H), 7.20 (d, J = 9.0 Hz, 1H), 6.91 (dd, J = 7.6, 1.9 Hz, 1H), 6.85 (dd, J = 13.9, 11.0 Hz, 2H), 4.54 (s, 4H), 3.90 (s, 3H).

H_2L (7.61 mg, 0.02 mmol) was dissolved in a chloroform/ethanol (vol/vol, 1:4) mixed solution (5 mL) and after stirring for 10 min, the solution was filtered; the filtrate was moved to a bottle which was sealed with foil, and after standing at room temperature for about one week, colorless transparent block-shaped crystals suitable for X-ray diffraction analysis were obtained with a yield of 46.2%.

2.3. Syntheses of H_2L and its Cu(II) complex

Synthetic route to the Cu(II) complex is described in Scheme 2.

To a methanol solution (3 mL) of $Cu(ClO_4)_2 \cdot 6H_2O$ (7.41 mg, 0.02 mmol) was added dropwise a solution of H_2L (7.61 mg, 0.02 mmol) in 3 mL of acetone. After mixing, it turned into a clear brown solution immediately and was stirred at room temperature



Scheme 2. Synthetic route to the Cu(II) complex.

for 5 min. The solution was filtered to remove the impurities, the bottle was sealed with foil, and let it sit for one week to evaporate. A brown block-shaped single crystal suitable for X-ray diffraction analysis was obtained. Yield: 40.52%. Anal. Calcd for [Cu₂(L)₂] (C₄₂H₃₆Cu₂N₄O₁₀) (%): C, 57.02; H, 4.07; N, 6.34; Cu, 14.38. Found: C, 57.31; H, 4.23; N, 6.06; Cu, 14.12.

2.4. X-ray structure determinations of H₂L and its Cu(II) complex

Crystal data of H₂L and its Cu(II) complex were obtained via a Bruker Smart Apex CCD diffractometer at 100.03(10) K and 293(2) K (Cu K α and Mo K α radiation ($\lambda = 1.54178$ and 0.71073 Å)), respectively [68]. The cell parameters of H₂L and its Cu(II) complex were determined by the least squares method. The LP calibration was used in SCALE3 program, while semi-empirical calibration was used in SADABS. The structures were analyzed by direct methods (SHELXS-2015). All non-hydrogen atoms were refined by full matrix least squares anisotropy. The positions of hydrogens were calculated and fixed isotropically in the final refinement. The key crystal data and structural parameters of H₂L and its Cu(II) complex are summarized in Table 1.

3. Results and discussion

3.1. IR spectral analyses

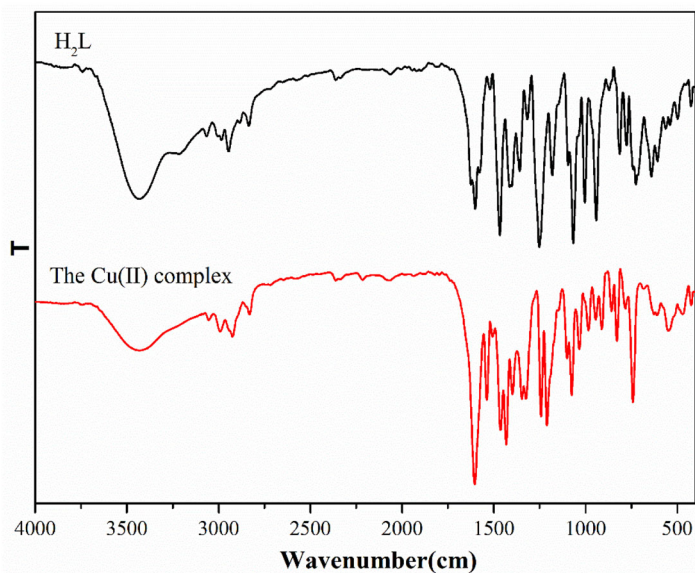
IR spectra of H₂L and its Cu(II) complex exhibits different bands from 4000 to 400 cm⁻¹ (Table 2 and Figure 1). The characteristic absorption band of the hydroxyl group of H₂L appears at *ca.* 3436 cm⁻¹, while that of the Cu(II) complex is obviously weakened, which is due to deprotonation of H₂L and coordination to Cu(II) [39]. Free H₂L exhibits the characteristic C=N stretching band at *ca.* 1599 cm⁻¹, and the Cu(II) complex shows that the C=N stretch occurred about 3 cm⁻¹ lower [43]. Meanwhile,

Table 1. Crystallographic data and refinement parameters for H₂L and its Cu(II) complex.

Compound	H ₂ L	Cu(II) complex
Empirical formula	C ₂₁ H ₂₀ N ₂ O ₅	C ₄₂ H ₃₆ Cu ₂ N ₄ O ₁₀
Molecular weight	380.39	883.83
Crystal size (mm)	0.12 × 0.10 × 0.08	0.12 × 0.11 × 0.10
Habit	Block-shaped	Block-shaped
Crystal system	Monoclinic	Monoclinic
Space group	<i>C1₂/c1</i>	<i>P1₂₁/c1</i>
Unit cell dimensions		
<i>a</i> (Å)	28.326(3)	8.4428(6)
<i>b</i> (Å)	4.8427(5)	28.839(3)
<i>c</i> (Å)	25.901(2)	7.6170(9)
α (°)	90	90
β (°)	93.106(9)	105.309(10)
γ (°)	90	90
<i>V</i> (Å ³)	3547.7(6)	1788.8(3)
<i>Z</i>	8	2
<i>D</i> _{calc} (g cm ⁻³)	1.424	1.641
μ (mm ⁻¹)	0.849	1.260
<i>F</i> (000)	1600	908
θ range for data collection (°)	3.125–73.398	2.501–29.590
Index ranges	$-30 \leq h \leq 34$, $-2 \leq k \leq 5$, $-31 \leq l \leq 30$	$-10 \leq h \leq 10$, $-36 \leq k \leq 37$, $-10 \leq l \leq 10$
Reflections collected	5753	9023
Completeness to theta (%)	97.4	83.2
Data/restraints/parameters	3456/0/256	4191/0/263
Final <i>R</i> ₁ , <i>wR</i> ₂ indices	0.0901, 0.2055	0.0727, 0.1031
<i>R</i> ₁ , <i>wR</i> ₂ indices (all data)	0.1559, 0.2743	0.0936, 0.1111
Largest diff. peak and hole (e·Å ⁻³)	0.275, -0.445	0.547, -0.634

Table 2. The major IR spectral data of H₂L and its Cu(II) complex (cm⁻¹).

Compound	ν (O-H)	ν (C=N)	ν (Ar-O)	ν (M-O)	ν (M-N)
H ₂ L	3436	1599	1258	–	–
Cu(II) complex	–	1596	1249	465	547

**Figure 1.** Infrared spectra of H₂L and its Cu(II) complex.

the Ar–O stretch of H₂L is observed at 1258 cm⁻¹, while that of the Cu(II) complex appears at 1249 cm⁻¹. A displacement of 9 cm⁻¹ may be due to formation of Cu–O bonds between the Cu(II) ion and the deprotonated L²⁻ [44].

In order to determine the frequency of Cu–O and Cu–N bonds, the far-IR spectra of the Cu(II) complex was obtained from 500 to 100 cm⁻¹. The Cu–O and Cu–N vibration frequencies was observed at 467 and 547 cm⁻¹. The above experimental results indicate that Cu(II) ion is coordinated to the N- and O-donors of L²⁻.

3.2. UV-vis absorption spectral analyses

The UV-vis absorption spectra of H₂L and its Cu(II) complex in ethanol (1.0 × 10⁻⁵ mol L⁻¹) at 298 K are shown in Figure 2(a). The absorptions of free H₂L and its Cu(II) complex are significantly different. The free H₂L shows absorption peaks at 268, 301, 313, 339, and 355 nm. The absorption peak at 268 nm can be attributed to the π–π* transition of benzene ring of H₂L, and the absorption peaks at 301 and 313 nm can be assigned to the π–π* transition of the naphthalene ring of H₂L [47]. The absorption peaks at 339 and 355 nm can be assigned to the n–π* transition of oxime nitrogen of H₂L [49]. Compared with H₂L, the four absorptions at 268, 301, 339, and 355 nm disappear in the UV-vis spectrum of the Cu(II) complex, the peak at 313 nm assigned to the π–π* transition of naphthalene ring is shifted to 315 nm, and a new absorption appears at 381 nm, which can be attributed to the L→M (LMCT) charge transition, which is characteristic of transition metal complexes with N₂O₂ coordination sphere [50].

A UV-vis titration experiment was performed (Figure 2(b)). When 1.0 equivalent of Cu(II) ion was added dropwise to solution of H₂L, the absorption peak at 381 nm reached the maximum value and no longer changed. This is consistent with the UV-vis spectrum of the Cu(II) complex. The titration spectra data show that the ratio of the replacement reaction is 1:1 ([Cu²⁺]/[H₂L]).

3.3. Description of the crystal structures of H₂L and its Cu(II) complex

3.3.1. Crystal structure of H₂L

The molecular structure of H₂L is shown in Figure 3(a). H₂L crystallizes in the monoclinic space group *C*1₂/*c*1. X-ray crystallography clearly shows that H₂L exhibits a V-shaped structure (N1–O2–C16–C15–O1–N2). In addition, H₂L has two important intramolecular O3–H3···N1 and O4–H4···N2 hydrogen bond interactions (Figure 3(b)), and an intermolecular C4–H4A···O2 hydrogen bond interaction (Figure 3(c)). Through the interactions of intermolecular hydrogen bonds, H₂L molecules form a 1-D chain structure (Figure 3(d)).

3.3.2. Crystal structure of the Cu(II) complex

The crystal structure and coordination configuration of the Cu(II) complex are shown in Figure 4. Significant bond lengths and angles are summarized in Table 3. Obviously, the Cu(II) complex has a symmetric dinuclear structure. The Cu(II) complex crystallizes in the monoclinic crystal system *P*1₂₁/*c*1 space group. This special structure of the

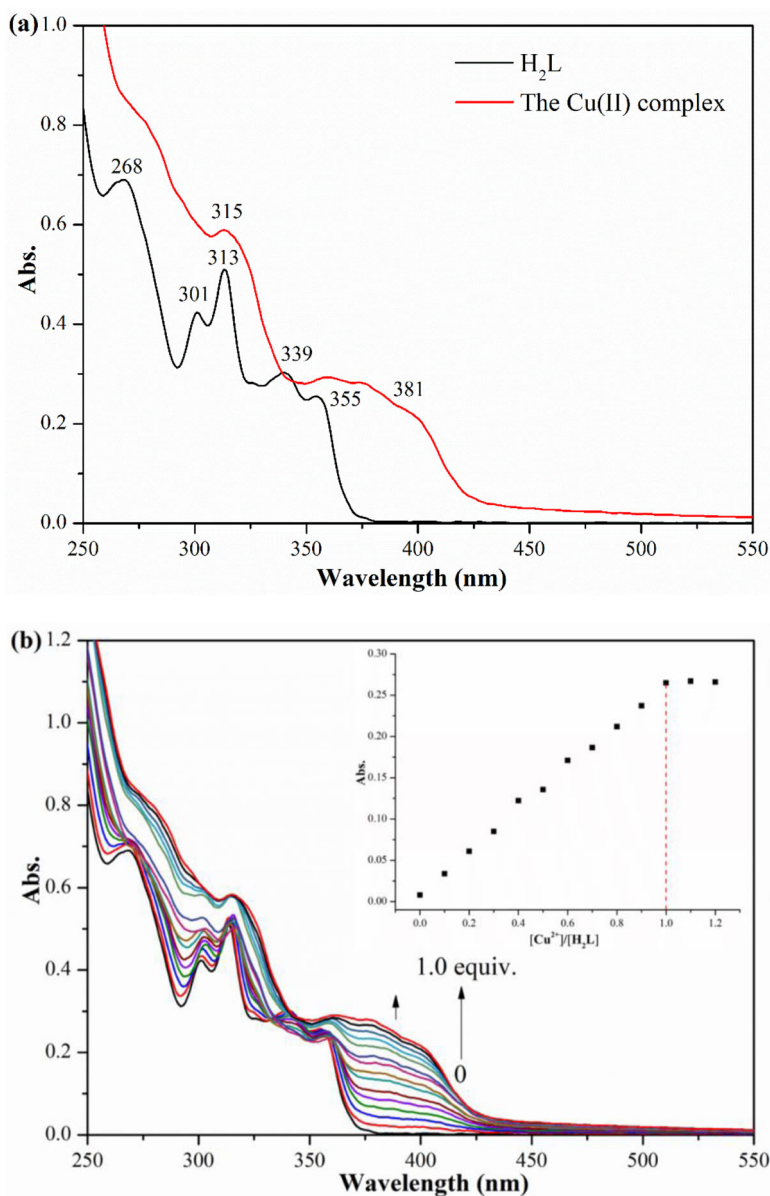


Figure 2. (a) UV-vis spectra of H_2L and its $Cu(II)$ complex ($c = 1.0 \times 10^{-5} \text{ mol L}^{-1}$). (b) UV-vis spectral changes of H_2L upon addition of the $Cu(II)$ ions (CH_3CH_2OH , $1.0 \times 10^{-5} \text{ mol L}^{-1}$, $0 \leq [Cu^{2+}]/[H_2L] \leq 1.2$).

$Cu(II)$ complex is neither the common structures of 1:1 [51] and 3:2 [37] (M:L) reported in the literature, nor the formation of previously reported 2:2 (M:L) structure [40] (Scheme 2). The complex consists of two $Cu(II)$ ions and two fully deprotonated L^{2-} units. The two $Cu(II)$ ions have the same coordination environments. The five-coordinate $Cu(II)$ ($Cu1$) is located at the N_2O_2 cavity ($N1$, $N2$, $O1$, and $O4$) of the fully deprotonated L^{2-} unit. The four donors ($N1$, $N2$, $O1$, and $O4$) form a twisted equatorial plane,

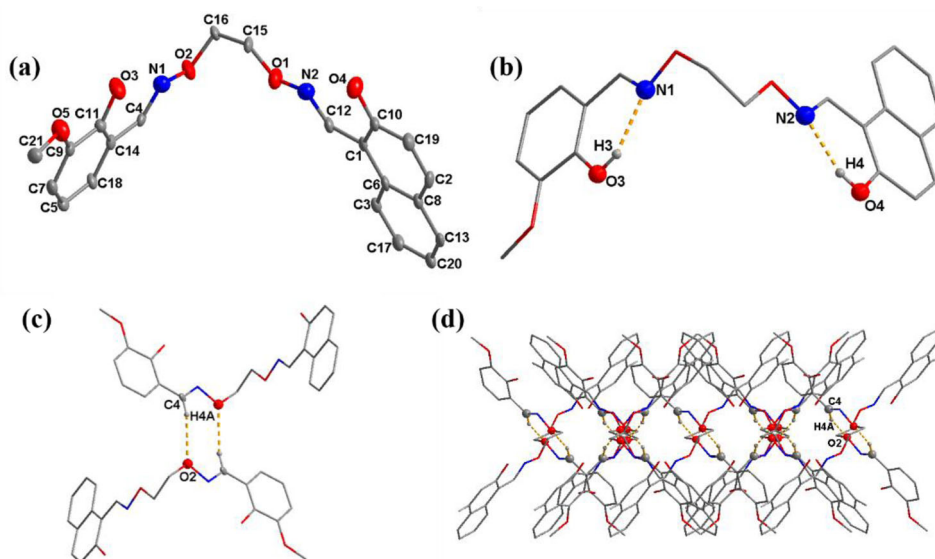


Figure 3. (a) The X-ray crystal structure of H₂L (hydrogens are omitted for clarity). (b) Intramolecular hydrogen bondings of H₂L. (c) Intermolecular hydrogen bonding of H₂L. (d) A 1-D chain structure is formed by intermolecular hydrogen bonding.

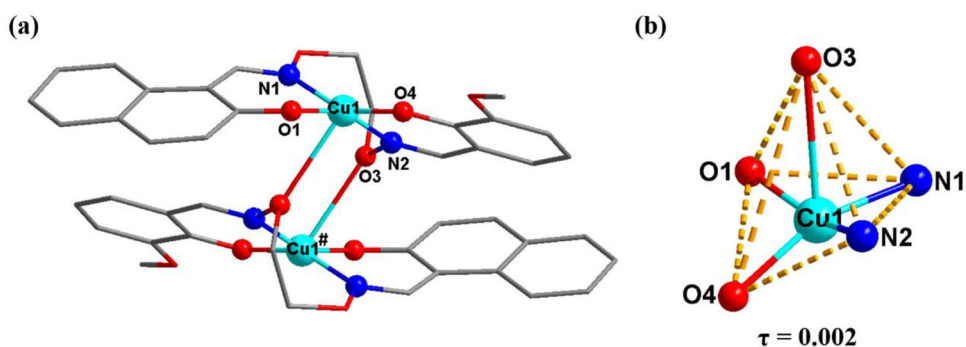


Figure 4. (a) The crystal structure of the Cu(II) complex (hydrogens are omitted for clarity). (b) Coordination configuration for Cu(II) ions of the Cu(II) complex.

Table 3. Selected bond lengths (Å) and angles (°) for the Cu(II) complex.

Bond	Lengths	Bond	Lengths
Cu1-O1	1.892(3)	Cu1-N1	1.989(3)
Cu1-O3	2.838(2)	Cu1-N2	1.918(3)
Cu1-O4	1.923(3)		
Bond	Angles	Bond	Angles
O1-Cu1-O3	143.32(10)	O3-Cu1-N1	74.46(9)
O1-Cu1-O4	89.55(12)	O3-Cu1-N2	26.88(11)
O1-Cu1-N1	91.82(12)	O4-Cu1-N1	155.04(12)
O1-Cu1-N2	156.35(13)	O4-Cu1-N2	90.38(13)
O3-Cu1-O4	117.15(10)	N1-Cu1-N2	98.07(12)

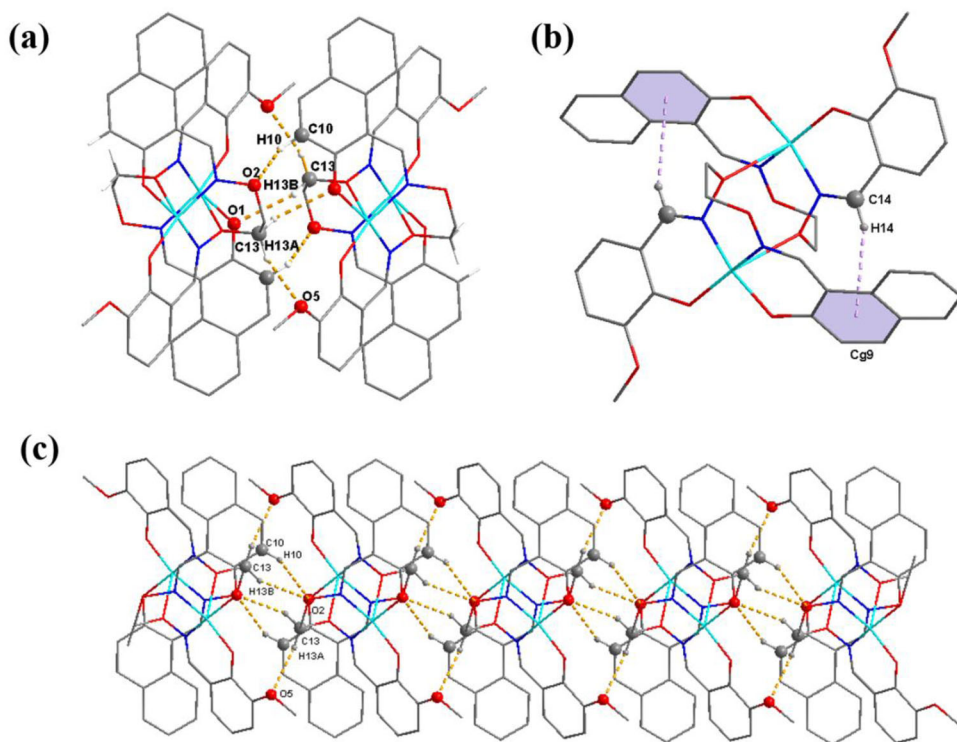


Figure 5. (a) The intermolecular hydrogen bonding interactions of the Cu(II) complex (hydrogens are omitted for clarity). (b) The C–H...Cg9 interaction of the Cu(II) complex. (c) The Cu(II) complex molecules formed a 1-D chain structure through intermolecular hydrogen bonding interactions.

where the dihedral angle of N1–Cu1–O1 and N2–Cu1–O4 planes is about $33.70(2)^\circ$ and the axial position is occupied by the oxime oxygen (O3) of another L^{2-} unit. Therefore, the Cu1 ion has a slightly twisted tetragonal pyramid geometry with $\tau = 0.002$ [39].

In the crystal structure of the Cu(II) complex, there are three pairs of intermolecular hydrogen bonds (C10–H10...O2, C13–H13A...O5, C13–H13B...O1) [36, 42, 49, 54], as shown in Figure 5(a). The Cu(II) complex also has C14–H14...Cg9 interaction, as shown in Figure 5(b). In addition, in Figure 5(c), a 1-D chain structure can be formed by intermolecular hydrogen bonding interactions.

3.4. Hirshfeld surfaces analyses

Hirshfeld surface analysis can investigate interactions between molecules in certain positions in the crystal environment, and can also clearly give the interface of the interaction between molecules, and judge the type of interaction from the color of different areas of the interface [39, 54]. The results of Hirshfeld surface analyses of H_2L and its Cu(II) complex are shown in Figure 6. The difference in surface shape of Hirshfeld plot reveals the degree of intermolecular bonding in the Cu(II) complex. There are red concave surfaces and blue convex surfaces in complementary regions of

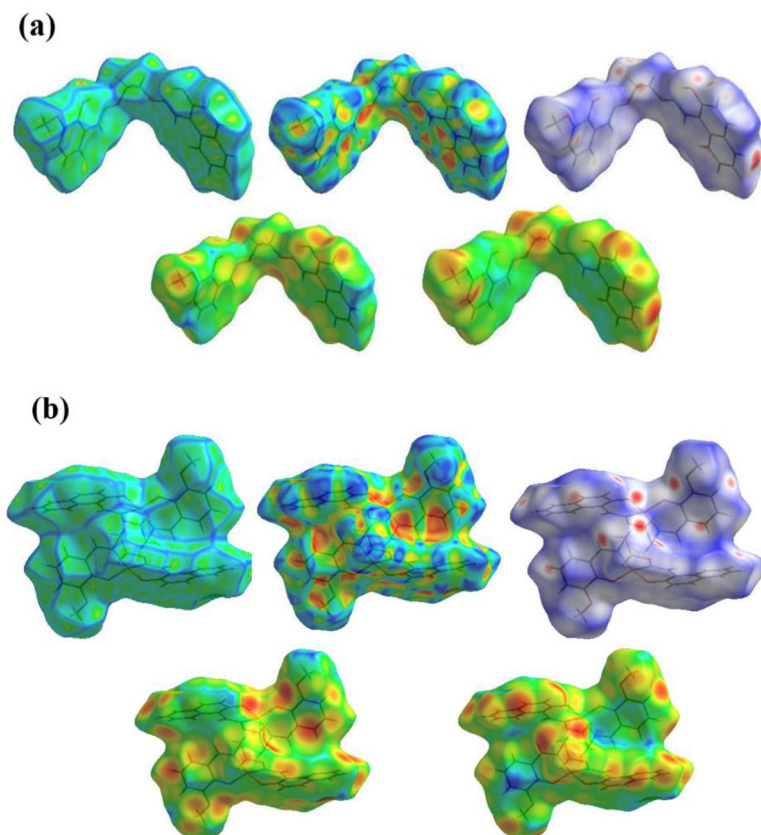


Figure 6. Hirshfeld surface analyses mapped with curvedness, shape-index, d_{norm} , d_e , and d_i of H_2L and its $Cu(II)$ complex.

H_2L and its $Cu(II)$ complex. The red concave surfaces can be attributed to $C-H\cdots O$ interactions, and the blue convex surfaces represent the $C\cdots H$, $H\cdots H$ and $C\cdots C$ contacts. In the d_{norm} of Hirshfeld surface analyses mapped, the white areas present on the surface are due to the longer distance between the molecules, not the existence of hydrogen bonds.

The generated 2-D map corresponds to the interactions between $O\cdots H$, $C\cdots H$, and $H\cdots H$ in H_2L and its $Cu(II)$ complex. Most of the fingerprints are occupied by gray areas, and blue areas indicate different degrees of interaction between molecules, as shown in Figure 7. In H_2L , the interactions of $C-H/H-C$, $O-H/H-O$, and $H-H/H-H$ accounted for 24.4%, 21.0%, and 44.1% of the total ligand Hirshfeld surfaces. In the $Cu(II)$ complex, the proportion of interaction of $C-H/H-C$ (27.3%) and $H-H/H-H$ (45.9%) is obviously increased, and the increase of weak molecular interactions also indicated that the $Cu(II)$ complex is stable. The interaction of $O-H/H-O$ (19.9%) decreased, which is attributed to deprotonation of phenolic hydroxyl groups and coordination with $Cu(II)$. The increase of hydrogen bonds also indicates that the $Cu(II)$ complex is stable, consistent with the results of the crystal structure description.

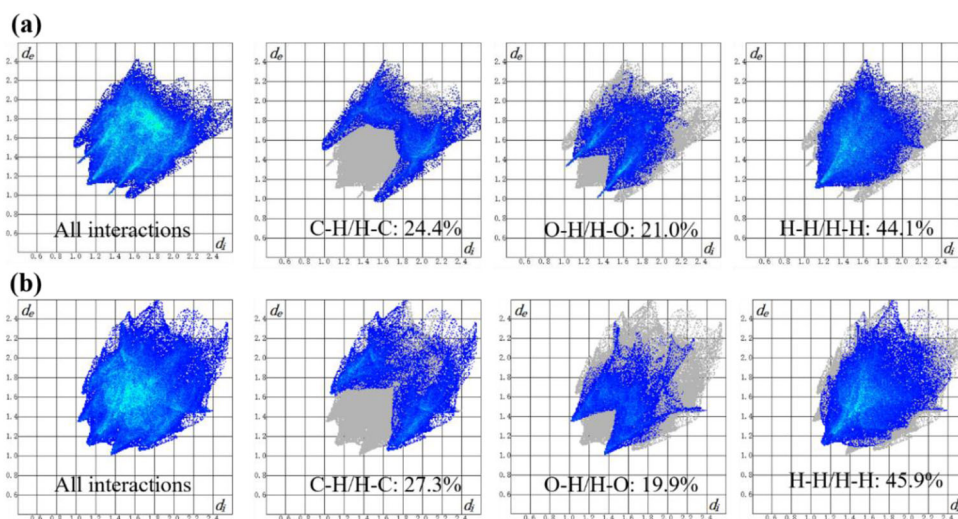


Figure 7. Fingerprint plots of H_2L and its $\text{Cu}(\text{II})$ complex: resolved into $\text{C}\cdots\text{H}$, $\text{O}\cdots\text{H}$, and $\text{H}\cdots\text{H}$ contacts showing the percentages of contacts contributed to the total Hirshfeld surface area of molecule.

3.5. Fluorescence properties

At room temperature, the fluorescence properties of H_2L and its $\text{Cu}(\text{II})$ complex were investigated in ethanol solution ($1.0 \times 10^{-4} \text{ mol L}^{-1}$). The excitation wavelength is 330 nm and the slit width is 10/20 nm. As shown in Figure 8(a), H_2L shows a strong fluorescence emission peak at 395 nm, attributed to the $\pi\text{-}\pi^*$ transition of the ligand. Compared with H_2L , the fluorescence of the $\text{Cu}(\text{II})$ complex is quenched, which indicates that the $\text{Cu}(\text{II})$ ion is coordinated with L^{2-} , thereby reducing the conjugated system.

A titration experiment of the binding affinity of $\text{Cu}(\text{II})$ ions to H_2L was also conducted (Figure 8(b)). With gradual addition of $\text{Cu}(\text{II})$ ions, the fluorescence intensity gradually weakened until the amount of $\text{Cu}(\text{II})$ ions added reached 1.0 equivalent; the fluorescence of the solution was completely quenched and no longer changed. It was further confirmed that the coordination ratio of H_2L to $\text{Cu}(\text{II})$ ions is 1:1. The Job working curve (illustration) is consistent with the above experimental results. According to the Benesi–Hildebrand formula (Figure 8(c)) [58, 69], the binding constant K of H_2L and $\text{Cu}(\text{II})$ ions is estimated to be $4.65 \times 10^6 \text{ M}^{-1}$.

4. Conclusion

A rare $\text{Cu}(\text{II})$ complex $[\text{Cu}_2(\text{L})_2]$ based on a new asymmetric salamo-based H_2L was obtained. H_2L formed a 1-D chain structure through intermolecular hydrogen bonding interactions. For the $\text{Cu}(\text{II})$ complex, the $\text{Cu}(\text{II})$ ions are coordinated with the N_2O_2 cavity (N1, N2, O1, and O4) and the oxime oxygen (O3) of another L^{2-} unit to form a slightly distorted five-coordinate tetragonal pyramid configuration, and through intermolecular interactions form a 1-D chain structure. Hirshfeld surface analyses further confirmed the intermolecular interactions in H_2L and its $\text{Cu}(\text{II})$ complex. Compared

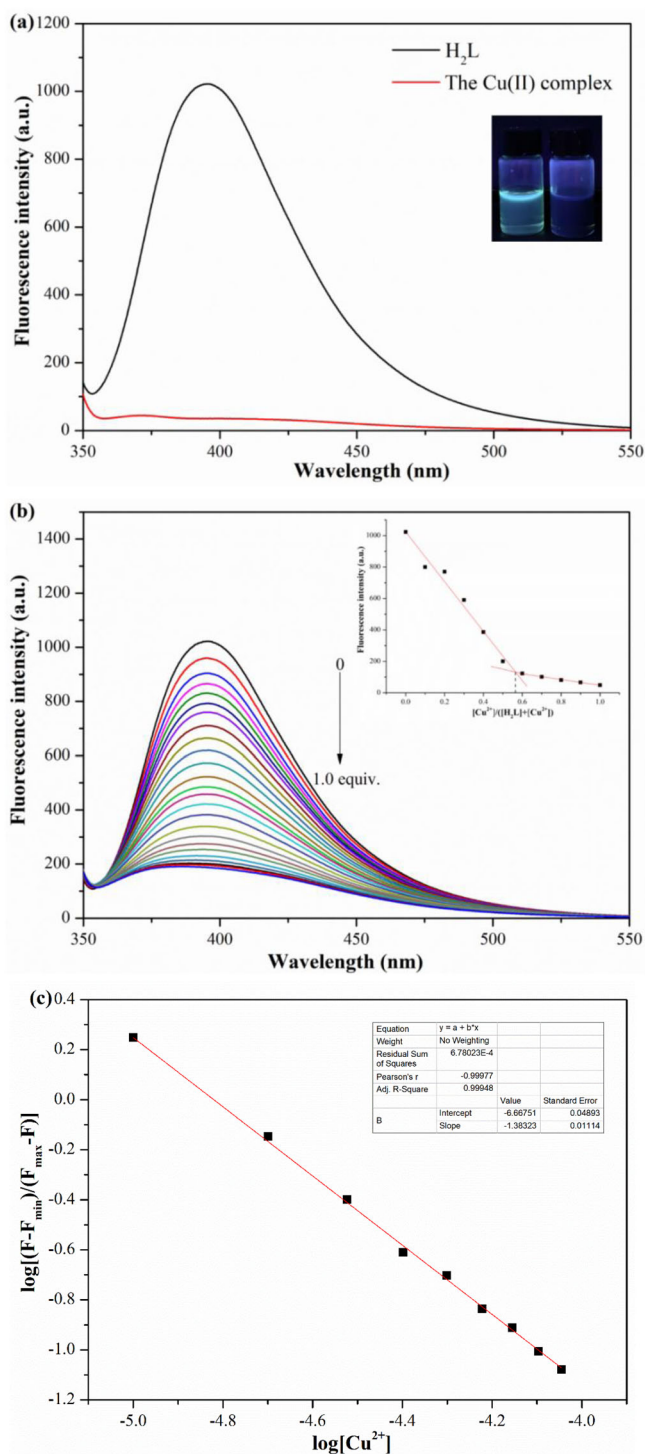


Figure 8. (a) Emission spectra of H_2L and its $Cu(II)$ complex ($c = 1.0 \times 10^{-4} \text{ mol L}^{-1}$). (b) Fluorescence titration spectra of H_2L with $Cu(II)$ ions. (c) Binding constant K of H_2L with $Cu(II)$ ions.

with H₂L, the fluorescence of the Cu(II) complex quenches, which is due to the formation of a more stable complex by Cu(II) ion coordination.

Disclosure statement

No potential conflict of interest was reported by the authors.

Funding

This work was supported by the National Natural Science Foundation of China (21968032) and the Program for Excellent Team of Scientific Research in Lanzhou Jiaotong University (201706), which are gratefully acknowledged.

References

- [1] F. Zhou, S.L. Xie, X.T. Gao, R. Zhang, C.H. Wang, G.Q. Yin, J. Zhou. *Green Chem.*, 19, 3908 (2017).
- [2] C. Chen, W.B. Wu, Y.H. Li, Q.H. Zhao, J.S. Yu, J. Zhou. *Org. Lett.*, 22, 2099 (2020).
- [3] H. Asaba, T. Iwasaki, M. Hatazawa, J. Deng, H. Nagae, K. Mashima, K. Nozaki. *Inorg. Chem.*, 59, 7928 (2020).
- [4] A. Gualandi, M. Marchini, L. Mengozzi, H.T. Kidanu, A. Franc, P. Ceroni, P.G. Cozzi. *Eur. J. Org. Chem.*, 2020, 1486 (2020).
- [5] H. Reiss, H. Shalit, V. Vershinin, N.Y. More, H. Forckosh, D. Pappo. *J. Org. Chem.*, 84, 7950 (2019).
- [6] S. Akine, M. Miyashita, T. Nabeshima. *Chem. Eur. J.*, 25, 1366 (2019).
- [7] K. Hemmat, M.A. Nasser, A. Allahresani. *ChemistrySelect*, 4, 4339 (2019).
- [8] M.R. Chiong, F.N.C. Paraan. *RSC Adv.*, 9, 23254 (2019).
- [9] A. Tzubery, N. Melamed-Book, E.Y. Tshuva. *Dalton Trans.*, 47, 3669 (2018).
- [10] W.H. Woo, K. Hyun, Y. Kim, J.Y. Ryu, J. Lee, M. Kim, M.H. Park, Y. Kim. *Eur. J. Inorg. Chem.*, 2017, 5372 (2017).
- [11] X. Xia, C. Lu, B. Zhao, Y. Yao. *RSC Adv.*, 9, 13749 (2019).
- [12] A. Sumiyoshi, Y. Chiba, R. Matsuoka, T. Noda, T. Nabeshima. *Dalton Trans.*, 48, 13169 (2019).
- [13] M. Novozhilova, D. Anischenko, I. Chepurnaya, E. Dmitrieva, V. Malev, A. Timonov, M. Karushev. *Electrochim. Acta*, 353, 136496 (2020).
- [14] M. Yamamura, H. Takizawa, N. Sakamoto, T. Nabeshima. *Tetrahedron Lett.*, 54, 7049 (2013).
- [15] W. Fu, Y. Pi, M. Gao, W. Wang, C. Li, R. Tan, D. Yin. *Chem. Commun. (Camb.)*, 56, 5993 (2020).
- [16] C.K. Ng, R.W. Toh, T.T. Lin, H.K. Luo, T.S.A. Hor, J. Wu. *Chem. Sci.*, 10, 1549 (2019).
- [17] S.W. Kwak, H. Jin, J.H. Lee, H. Hwang, M. Kim, Y. Kim, Y. Chung, K.M. Lee, M.H. Park. *Inorg. Chem.*, 58, 2454 (2019).
- [18] D. Park, C.I. Jette, J. Kim, W.O. Jung, Y. Lee, J. Park, S. Kang, M.S. Han, B.M. Stoltz, S. Hong. *Angew. Chem. Int. Ed. Engl.*, 59, 775 (2020).
- [19] Y. Tong, B. Liu, Y. Wu, B. Yang, G. Wen, Y.T. Yang, J. Chai, X. Hu. *Sens. Actuators B: Chem.*, 252, 794 (2017).
- [20] K.K. Xu, G.M. Xia, D. Liu, L.X. Jiang, M.D. Wang, D.J. Liu, X. Lv, W.Z. Shan, H.M. Wang. *J. Polym. Sci. Part A: Polym. Chem.*, 57, 641 (2019).
- [21] M.B. Solomon, A. Rawal, J.M. Hook, S.M. Cohen, C.P. Kubiak, K.A. Jolliffe, D.M. D'Alessandro. *RSC Adv.*, 8, 24128 (2018).
- [22] S. Mirza, H. Chen, S.M. Chen, Z.G. Gu, J. Zhang. *Cryst. Growth Des.*, 18, 7150 (2018).
- [23] M.H. Khan, M. Cai, J. Deng, P. Yu, H. Liang, F. Yang. *Molecules*, 24, 2544 (2019).

- [24] M. Umemura, M.R. Islam, H. Fukumura, I. Sato, Y. Kawabata, K. Matsuo, R. Nakakaji, A. Nagasako, M. Ohtake, F. Takayuki, U. Yokoyama, T. Nakayama, H. Eguchi, Y. Ishikawa. *Cancer Sci.*, 110, 356 (2019).
- [25] C.B. Li, Y. Chu, J. He, J. Xie, J. Liu, N. Wang, J. Tang. *ChemCatChem*, 11, 6324 (2019).
- [26] S. Akine, H. Nagumo, T. Nabeshima. *Dalton Trans.*, 42, 15974 (2013).
- [27] J.C. Pessoa, I. Correia. *Coord. Chem. Rev.*, 388, 227 (2019).
- [28] T. Nakamura, Y. Kawashima, E. Nishibori, T. Nabeshima. *Inorg. Chem.*, 58, 7863 (2019).
- [29] D. Yuan, N. Cai, J. Xu, D. Miao, S. Zhang, S.E. Woodfine, D. Plana, C.S. Hawes, M. Watkinson. *Chempluschem*, 85, 1210 (2020).
- [30] T. Nakamura, S. Tsukuda, T. Nabeshima. *J. Am. Chem. Soc.*, 141, 6462 (2019).
- [31] A. Antalík, L. Veis, J. Brabec, O. Demel, O. Legeza, J. Pittner. *J. Chem. Phys.*, 151, 084112 (2019).
- [32] Y. Ning, Y. Huo, H. Xue, Y. Du, Y. Yao, A.C. Sedgwick, H. Lin, C. Li, S.D. Jiang, B.W. Wang, S. Gao, L. Kang, J.L. Sessler, J.L. Zhang. *J. Am. Chem. Soc.*, 142, 10219 (2020).
- [33] M. Saikawa, T. Noda, R. Matsuoka, T. Nakamura, T. Nabeshima. *Eur. J. Inorg. Chem.*, 2019, 766 (2019).
- [34] S. Akine, M. Miyashita, S. Piao, T. Nabeshima. *Inorg. Chem. Front.*, 1, 53 (2014).
- [35] Y. Zhang, M. Yu, Y.Q. Pan, Y. Zhang, L. Xu, X.Y. Dong. *Appl. Organomet. Chem.*, 34, e5442 (2020).
- [36] Z.L. Ren, J. Hao, P. Hao, X.Y. Dong, Y. Bai, W.K. Dong. *Z. Naturforsch.*, 73, 203 (2018).
- [37] Y.Q. Pan, Y. Zhang, M. Yu, Y. Zhang, L. Wang. *Appl. Organomet. Chem.*, 34, e5441 (2020).
- [38] L.W. Zhang, Y. Zhang, Y.F. Cui, M. Yu, W.K. Dong. *Inorg. Chim. Acta*, 506, 119534 (2020).
- [39] C. Liu, X.X. An, Y.F. Cui, K.F. Xie, W.K. Dong. *Appl. Organomet. Chem.*, 34, e5272 (2020).
- [40] M. Yu, Y. Zhang, Y.Q. Pan, L. Wang. *Inorg. Chim. Acta*, 509, 119701 (2020).
- [41] L.Z. Liu, L. Wang, M. Yu, Q. Zhao, Y. Zhang, Y.X. Sun, W.K. Dong. *Spectrochim. Acta A Mol. Biomol. Spectrosc.*, 222, 117209 (2019).
- [42] X.Y. Dong, Q. Zhao, Q.P. Kang, X.Y. Li, W.K. Dong. *Crystals*, 8, 230 (2018).
- [43] X.X. An, Q. Zhao, H.R. Mu, W.K. Dong. *Crystals*, 9, 101 (2019).
- [44] Y.F. Cui, Y. Zhang, K.F. Xie, W.K. Dong. *Crystals*, 9, 596 (2019).
- [45] X.Y. Li, Q.P. Kang, C. Liu, Y. Zhang, W.K. Dong. *New J. Chem.*, 43, 4605 (2019).
- [46] Y. Zhang, L.Z. Liu, Y.D. Peng, N. Li, W.K. Dong. *Transit. Met. Chem.*, 44, 627 (2019).
- [47] Q.P. Kang, X.Y. Li, Z.L. Wei, Y. Zhang, W.K. Dong. *Polyhedron*, 165, 38 (2019).
- [48] Q. Zhao, X.X. An, L.Z. Liu, W.K. Dong. *Inorg. Chim. Acta*, 490, 6 (2019).
- [49] H.R. Mu, X.X. An, C. Liu, Y. Zhang, W.K. Dong. *J. Struct. Chem.*, 61, 1218 (2020).
- [50] L. Wang, Q.P. Kang, J. Hao, Y. Zhang, Y. Bai, W.K. Dong. *Chin. J. Inorg. Chem.*, 34, 525 (2018).
- [51] Q.P. Kang, X.Y. Li, L. Wang, Y. Zhang, W.K. Dong. *Appl. Organomet. Chem.*, 33, e5013 (2019).
- [52] M. Yu, H.R. Mu, L.Z. Liu, N. Li, Y. Bai, X.Y. Dong. *Chin. J. Inorg. Chem.*, 35, 1109 (2019).
- [53] L.Z. Liu, M. Yu, X.Y. Li, Q.P. Kang, W.K. Dong. *Chin. J. Inorg. Chem.*, 35, 1283 (2019).
- [54] X.Y. Dong, Q. Zhao, Z.L. Wei, H.R. Mu, H. Zhang, W.K. Dong. *Molecules*, 23, 1006 (2018).
- [55] H.R. Mu, M. Yu, L. Wang, Y. Zhang, Y.J. Ding. *Phosphorus Sulfur Silicon Relat. Elem.*, 195, 730 (2020).
- [56] Y.X. Sun, L.Z. Liu, F. Wang, X.Y. Shang, L. Chen, W.K. Dong. *Crystals*, 8, 227 (2018).
- [57] J. Chang, S.Z. Zhang, Y. Wu, H.J. Zhang, Y.X. Sun. *Transit. Met. Chem.*, 45, 279 (2020).
- [58] L. Wang, Z.L. Wei, Z.Z. Chen, C. Liu, W.K. Dong, Y.J. Ding. *Microchem. J.*, 155, 104801 (2020).
- [59] Y.Q. Pan, X. Xu, Y. Zhang, Y. Zhang, W.K. Dong. *Spectrochim. Acta A Mol. Biomol. Spectrosc.*, 229, 117927 (2020).
- [60] Z.L. Wei, L. Wang, J.F. Wang, W.T. Guo, Y. Zhang, W.K. Dong. *Spectrochim. Acta A Mol. Biomol. Spectrosc.*, 228, 117775 (2020).
- [61] X.X. An, Z.Z. Chen, H.R. Mu, L. Zhao. *Inorg. Chim. Acta*, 511, 119823 (2020).
- [62] X.X. An, C. Liu, Z.Z. Chen, K.F. Xie, Y. Zhang. *Crystals*, 9, 602 (2019).

- [63] L. Wang, Y.Q. Pan, J.F. Wang, Y. Zhang, Y.J. Ding. *J. Photochem. Photobiol. A*, 400, 112719 (2020).
- [64] C. Liu, Z.L. Wei, H.R. Mu, W.K. Dong, Y.J. Ding. *J. Photochem. Photobiol. A*, 397, 112569 (2020).
- [65] L. Wang, Z.L. Wei, C. Liu, W.K. Dong, J.X. Ru. *Spectrochim. Acta A Mol. Biomol. Spectrosc.*, 239, 118496 (2020).
- [66] Y.D. Peng, F. Wang, L. Gao, W.K. Dong. *J. Chin. Chem. Soc.*, 65, 893 (2018).
- [67] Y.X. Sun, Y.Q. Pan, X. Xu, Y. Zhang. *Crystals*, 9, 607 (2019).
- [68] G.M. Sheldrick. *SHELXL-2016, Program for Crystal Structure Refinement*, University of Göttingen, Göttingen Germany (2015).
- [69] S.Z. Zhang, J. Chang, H.J. Zhang, Y.X. Sun, Y. Wu, Y.B. Wang. *Chin. J. Inorg. Chem.*, 36, 503 (2020).